


Article

Amino-Modified Silica as Effective Support of the Palladium Catalyst for 4-Nitroaniline Hydrogenation

Adele R. Latypova ^{1,*}, Maxim D. Lebedev ¹, Evgeniy V. Rumyantsev ^{1,2}, Dmitry V. Filippov ¹, Olga V. Lefedova ¹, Alexey V. Bykov ³ and Valentin Yu. Doluda ^{1,3}

¹ Ivanovo State University of Chemistry and Technology, Sheremetevsky ave.7, 153000 Ivanovo, Russia; maxkys2@yandex.ru (M.D.L.); naturer@yandex.ru (E.V.R.); fillipov@isuct.ru (D.V.F.); physchem.606@yandex.ru (O.V.L.); doludav@yandex.ru (V.Y.D.)

² Federal State Budget Educational Institution of Higher Education «Ivanovo State Polytechnic University», Sheremetevsky ave. 21, 153000 Ivanovo, Russia

³ Tver State Technical University, Nab. A. Nikitina 22, 170042 Tver, Russia; bykovav@yandex.ru

* Correspondence: LatAdel@yandex.ru

Received: 4 March 2020; Accepted: 29 March 2020; Published: 31 March 2020



Abstract: The article describes the synthesis of aminoorgano-functionalized silica as a prospective material for catalysis application. The amino groups have electron donor properties which are valuable for the metal chemical state of palladium. Therefore, the presence of electron donor groups is important for increasing catalysts' stability. The research is devoted to the investigation of silica amino-modified support influence on the activity and stability of palladium species in 4-nitroaniline hydrogenation process. A series of catalysts with different supports such as SiO₂, SiO₂-C₃H₆-NH₂ (amino-functionalized silica), γ-Al₂O₃ and activated carbon were studied. The catalytic activity was studied in the hydrogenation of 4-nitroaniline to 1,4-phenylenediamine. The catalysts were characterized by scanning electron microscopy, transmission electron microscopy, X-ray photoelectron spectroscopy, Fourier transform infrared spectroscopy and chemisorption of hydrogen by the pulse technique. The 5 wt.% Pd/SiO₂-C₃H₆-NH₂ catalyst exhibited the highest catalytic activity for 4-nitroaniline hydrogenation with 100% conversion and 99% selectivity with respect to 1,4-phenylenediamine.

Keywords: sol-gel; amino-functionalized silica; catalyst; activity; hydrogenation

1. Introduction

Supported catalysts have wide applications in fine organic synthesis [1–4], industrial synthetic processes of petrochemicals [5–7] and pharmaceutical production [8–10]. However, in modern catalysis there is still the problem of increasing the activity and selectivity of catalysts, as well as the search for new catalytically active materials [11–16].

Possible ways to increase catalytic activity and selectivity include the development of catalysts synthesis methods, the optimization of reaction conditions, catalyst modification by different chemical elements and compounds, the application of supports and modification of the catalyst surface [4,11–14,16–20]. Modification of catalyst support surface is one possible solution to increase catalysts' activity and stability. The presence of functional groups on the support surface has great influence on the electronic state of active metal and metal dispersion [21]. The aminopropyl groups provide a unique possibility for further surface modification. Amino groups' modified supports are very useful for further surface nucleophilic substitution and obtaining the highest metal dispersion and study of this effect is a sufficiently novel trend in catalysis [4,19,20,22–25]. A lot of articles are dedicated to the application of amino-functionalized mesoporous silica in medicine, pharmaceuticals and smart materials, however, publications on their influence on active metals' catalytic properties

are fragmental [26–31]. The present study reports the synthesis of aminoorgano-functionalized silica immobilized by palladium nanoparticles using the sol-gel method. This allows the synthesization of various hybrid composition materials by the one-pot method. For comparison, amorphous silica, activated carbon and gamma-alumina were used as supports for palladium particles.

The catalytic activity of synthesized catalysts was tested in 4-nitroaniline hydrogenation (Figure 1). Liquid phase hydrogenation of substituted nitrobenzenes is an essential technology for the production of various aromatic amines—key intermediates for manufacturing agrochemicals, isocyanates, pharmaceuticals and dyes [32–35]. The most commonly used catalysts for different hydrogenation processes contain platinum group metals (palladium, platinum, iridium, etc.) attached to different supports [33–38]. Palladium nanoparticles were found to be the most active and have a high potential for the catalytic application of essential chemical products [33–35]. However, the catalysts' stability is an open issue for such types of catalyst, therefore the development of active and stable catalysts is the focus of the current article.

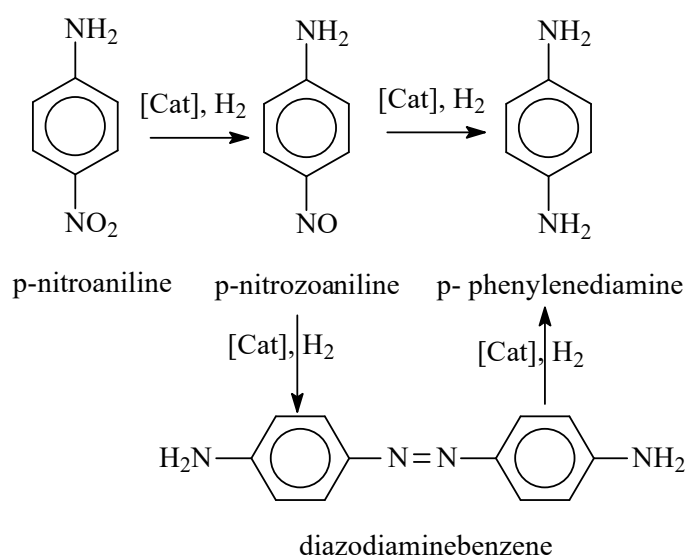


Figure 1. The scheme of 4-nitroaniline hydrogenation to 1,4 phenylenediamine.

Compounds such as 4-nitroaniline are used as an industrial raw material to produce agricultural chemicals, rubber compounding agents, synthetic resin additives, polyamides, pharmaceuticals and dyes. The conductive polyamines can be used in electronics [39], and also as antioxidants and preservatives [40–42]. The polyamines can find a wide application in films, materials and membranes due to their biodegradable and electro-conductive properties.

2. Results and Discussion

2.1. FTIR Spectroscopy of Silica Supports

Silica modification with aminopropyl groups with an NH_2 content of 30 wt.% was verified by Fourier transform infrared spectroscopy (Figure 2). The analysis of the FTIR spectra of modified and pure supports revealed the broad bands centered around 3441 cm^{-1} and correspond to O–H groups' vibrations. On the other hand, the spectrum of amino-functionalized silic peaks at 2940 and 2886 cm^{-1} and is assigned to the C–H stretching vibrations of CH- and CH_2 - groups, which can be attributed to the incorporation of the amino group [22,43]. The peak of the C–N stretching vibration at 1140 cm^{-1} overlaps with the Si–O–Si stretching band in the range 1000 – 1200 cm^{-1} . The peak of the N–H stretching vibration at ~ 3295 and 3358 cm^{-1} overlaps with a wide peak of stretching vibration at O–H at 3080 cm^{-1} [22,43]. The intense bands appearing at 1059 and 1176 cm^{-1} were assigned to the asymmetric stretching vibrations Si–O–Si. The symmetric stretching vibrations of Si–O–Si, deformation vibrations of O–Si–O

and C-Si-O, and in-plane stretching vibrations Si-O can overlap in the 582, 814 and 953 cm^{-1} range. The bands of Si-O stretching vibrations give reason to suggest the existence of SiO_2 network defects. The band observed at 467 cm^{-1} is assigned to the plane-stretching vibrations of Si-C [43].

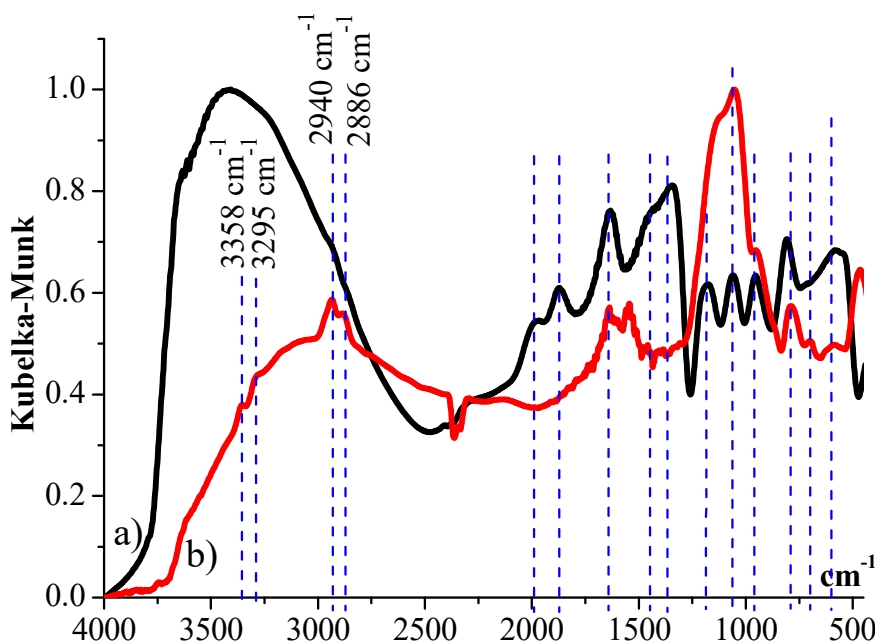


Figure 2. FTIR spectra of supports' surface: (a) SiO_2 ; (b) $\text{SiO}_2\text{-C}_3\text{H}_6\text{-(30\%)\text{NH}_2}$.

However, the use of tetraethoxysilane as a silica precursor led to the formation of surface methyl-functionalized silica. This was certified by a broad peak in the range 1338–1500 cm^{-1} which can be assigned to the C-H deformation vibrations of aliphatic bands [43].

2.2. The Pulse Chemisorption

The hydrogen pulse chemisorption data are presented in Table 1. Silica surface modification by tetraethoxysilane results in some increase in metal dispersion, and a concentration of active sites and a metallic surface area. However, metal dispersion remains considerably low.

Table 1. Hydrogen pulse chemisorption data.

Simple	Metal Dispersion, %	Metallic Surface Area, m^2/g Metal	Concentration of Active Center mmol/g
5 wt.% Pd/ $\text{SiO}_2\text{-C}_3\text{H}_6\text{-(30\%)\text{NH}_2}$	5.0	21	0.017
5 wt.% Pd/ SiO_2	4.3	19	0.016

2.3. XPS of Catalysts before the Reaction

The surface chemical composition of silica supports determined by X-ray photoelectron spectroscopy. The high-resolution XPS spectra of C 1s, N 1s, Si 2p are shown in the appropriate figure (Figure 3). According to XPS data, the silica contains O, C, Si elements. The synthesized amino-organomodified silica contains O, C, Si and N elements.

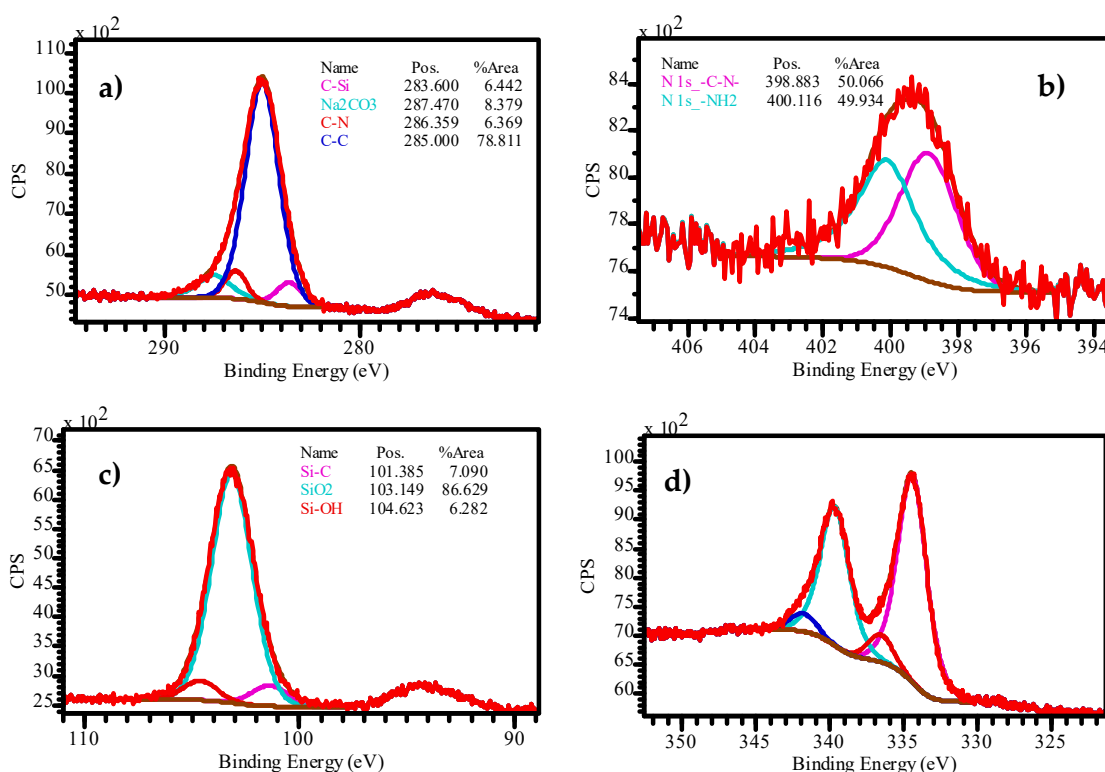


Figure 3. The high-resolution XPS spectra of (a) C 1s; (b) N 1s; (c) Si 2p; energy core-level of SiO₂-C₃H₆-(30%)NH₂ and (d) Pd 3d energy core-level of 5% wt. Pd/SiO₂-C₃H₆-(30%)NH₂.

The presence of quantities of aliphatic carbon compounds in silica is a result of the inclusion of an aminopropyl substituent in the silica structure, and the incomplete hydrolysis of silane and carbon pollution. The C-N and C-Si bonds prove the inclusion of aminopropyl substituents in the silicon oxide matrix. According to the published data [43,44], the peaks at 399.5 and 401.6 eV in the spectrum of N 1s can be attributed to C-N and N-H bonds that correlate with the IR-spectroscopy data (Figure 2) [43,44]. The bonds -C-ONa belong to molecules of sodium carbonate (Figure 3) [43,44].

Figure 3d shows the model decomposition of the XPS high-resolution spectra of Pd 3d energy core-level of 5% wt. Pd/SiO₂-C₃H₆-(30%)NH₂ catalyst before the reaction. The XPS data of the other catalysts were published in reference 52 of this paper. The atomic concentration of palladium compounds is given in Table 2. The model decomposition of Pd 3d spectra for 5 wt.% Pd/γ-Al₂O₃, 5 wt.% Pd/SiO₂, and 5 wt.% Pd/SiO₂-C₃H₆-(30%)NH₂ catalysts showed the presence of two palladium chemical states (Table 2, Figure 3d) [45]. Different states of palladium were observed in the catalyst of activated carbon, particularly metallic palladium Pd⁰, oxidized PdO on metallic Pd⁰ and palladium oxides PdO, PdO₂ [45].

Table 2. The spectrum data of catalysts before the reaction.

Catalyst	Binding Energy, eV	Chemical State	at, %
5 wt.% Pd/SiO ₂ [45]	334.87	Pd ⁰	1.47
	337.09	PdO	0.17
5 wt.% Pd/SiO ₂ -C ₃ H ₆ -NH ₂	334.44	Pd ⁰	2.12
	336.59	PdO/Pd ⁰	0.15

An interesting observation was a shift in the binding energy by ~0.5 eV of palladium metal in the 5 wt.% Pd SiO₂-C₃H₆-(30%)NH₂ catalyst in comparison to the standard binding energy of

metal palladium (335 eV). There was an assumption that this may be the result of the displacement of the electron cloud of amino groups to palladium atoms. This effect can take place in case of Pd nanoparticles' coordination by amino groups. A comparatively similar interaction between palladium nanoparticles and nitrogen-containing supports was reported in several articles devoted to palladium nanostructured materials synthesis and characterization [24,46,47]. Typically, a Pd charging by amino groups has a positive influence on hydrogen chemisorption on active metal that can have a positive effect on the hydrogenation of the substrate [24,46,47].

2.4. XPS of Used Catalysts

The atomic surface concentrations of palladium and palladium oxide decrease in 5 wt.% Pd/ γ -Al₂O₃, 5 wt.% Pd/SiO₂ and 5 wt.% Pd/C catalysts (Tables 2 and 3) which can be attributed to metal particles' diffusion into a matrix of support [45]. However, for amino-modified sample 5 wt.% Pd/SiO₂-C₃H₆-(30%)NH₂, a change in active metal surface concentration was not observed. The quantity of zero valence metal in 5 wt.% Pd/SiO₂ and 5 wt.% Pd/SiO₂-C₃H₆-(30%)NH₂ samples before and after reaction did not change significantly (Table 3). The changes in Pd⁰ surface concentrations in 5 wt.% Pd/C and Pd/ γ -Al₂O₃ catalysts were the most noticeable [45].

Table 3. The spectrum data of catalysts after used in reaction.

Catalyst	Binding Energy, eV	Chemical State	At, %
5 wt.% Pd/SiO ₂ [45]	335.04	Pd ⁰	1.04
	337.25	PdO	0.06
5 wt.% Pd/SiO ₂ -C ₃ H ₆ -(30%)NH ₂	334.51	Pd ⁰	2.10
	336.50	PdO/Pd ⁰	0.23

In the case of the 5 wt.% Pd/C catalyst, the quantity of PdO decreased on 0.7 at.% and the content of PdO₂ was increased on 0.7 at.% (Tables 2 and 3). The contents of PdO and Pd⁰ in 5 wt.% Pd/SiO₂ and 5 wt.% Pd/ γ -Al₂O₃ catalysts were decreased.

2.5. SEM

The morphology of the amino-functionalized mesoporous silica was studied by scanning electron microscopy (Figure 4). The synthesized silica particles have a spherical shape. Average particle size diameter was found to be 1 μ m before and after catalysts' synthesis.

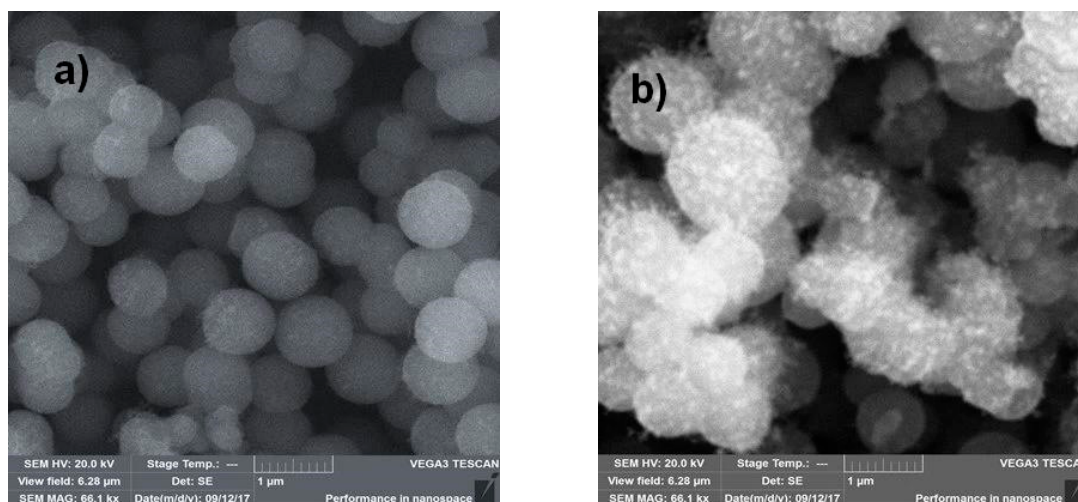


Figure 4. SEM images of (a) SiO₂-C₃H₆-(30%)NH₂ and (b) 5 wt.% Pd/SiO₂-C₃H₆-(30%)NH₂.

2.6. TEM

The images of transmission electron microscope were obtained for the reliable determination of palladium particle size (Figure 5). The images show that the particles are quite different in size.

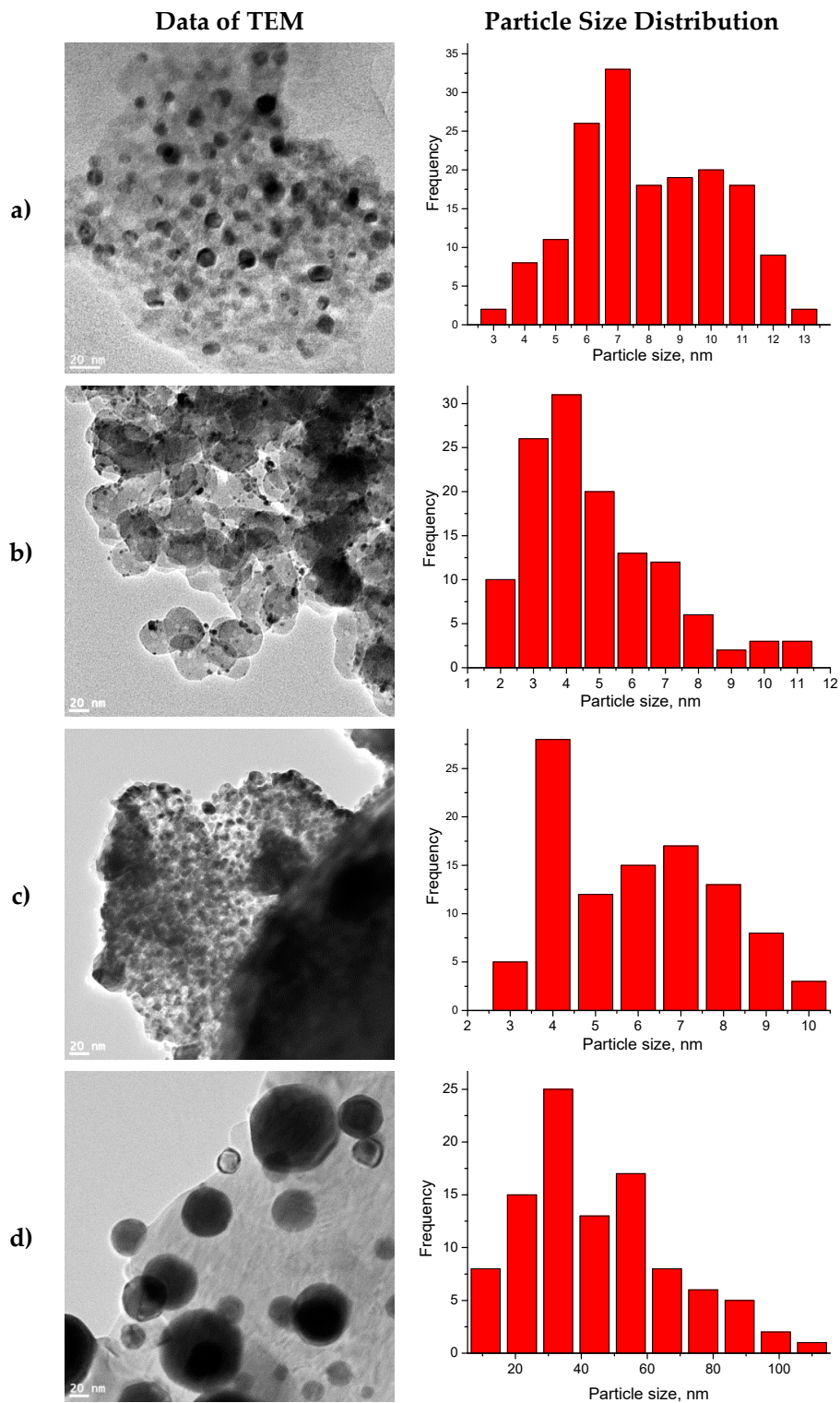


Figure 5. TEM images of catalysts and particle size distribution: (a) 5 wt.% Pd/ γ -Al₂O₃; (b) 5 wt.% Pd/SiO₂; (c) 5 wt.% Pd/SiO₂-C₃H₆-NH₂; (d) 5 wt.% Pd/C.

The particle size in the 5 wt.% Pd/SiO₂-C₃H₆-(30%)NH₂ catalyst varies from 3 to 10 nm; in the 5 wt.% Pd/SiO₂ catalyst, particle size varies from 2 to 10 nm; in the 5 wt.% Pd/ γ -Al₂O₃ catalyst, particle size varies from 5 to 70 nm; and in the 5 wt.% Pd/C catalyst, particle size varies from 30 to 100 nm. In general, the data agree with the result of hydrogen pulse chemisorption.

Depending on the size of the metal particles, according to both methods (microscopy and pulse chemisorption), the catalysts can be structured in the following row: 5 wt.% Pd/ γ -Al₂O₃ \approx 5 wt.% Pd/C > 5 wt.% Pd/SiO₂ > 5 wt.% Pd/SiO₂-C₃H₆-(30%)NH₂.

The TEM images with a high resolution were used to analyze the atomic lattice parameters of the catalytic phase. The interplanar distance of palladium particles in 5 wt.% Pd/ γ -Al₂O₃ is of the order of \sim 0.14 nm (220), which corresponds to the metallic palladium phase. Other palladium particles in 5 wt.% Pd/ γ -Al₂O₃ with an interplanar distance of about \sim 0.26 nm (111) belong to palladium oxide. The interplanar distances of \sim 0.14 nm (220) were observed for a catalyst of 5 wt.% Pd/SiO₂-C₃H₆-(30%)NH₂ [48–50]. The TEM data of 5 wt.% Pd/SiO₂ catalyst also show the interplanar spacings of \sim 0.14 (220) and \sim 0.26 nm (111) [48–50], which correspond to the metal and oxide state of palladium. The interplanar distances of \sim 0.14 (220) and \sim 0.26 nm (111) were observed for a catalyst of 5 wt.% Pd/C [48–50].

2.7. TPD of Matrices

According to the results of the TPD NH₃ study, the modification of silica by amino groups increased the amount of acid sites compared with silica (Figure 6).

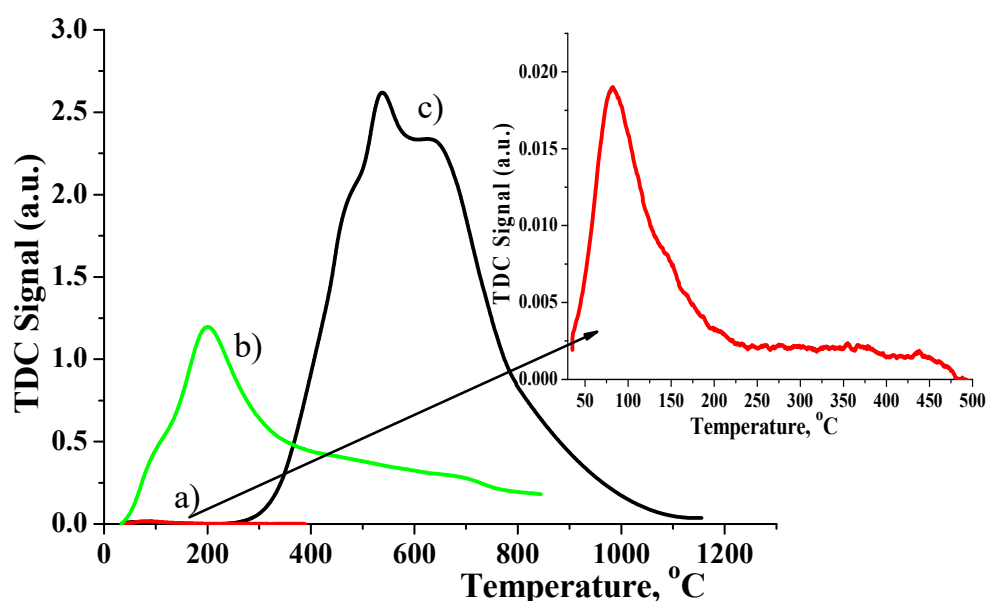


Figure 6. The acid properties of supports. The heating rate was 10 °C per minute. The composition of gas mixture is 3% NH₃ in He flow. (a) SiO₂, (b) γ -Al₂O₃, (c) SiO₂-C₃H₆-NH₂.

The alumina contains less acidic properties than amino-modified silica. Thus, according to the quantity and acid sites' strength, the catalyst supports can be given in the following order: SiO₂-C₃H₆-NH₂ > γ -Al₂O₃ > SiO₂.

2.8. The Activity of Synthesized Catalysts

In all cycles for all catalysts, the conversion of 4-nitroaniline to 1,4-phenylenediamine was 100%. A sufficient quantity of hydrogen for completely reduce to 4-nitroaniline is 3.62 mmol. Thus, according to the data of the catalysts, activity can arrange in the order: 5 wt.% Pd/SiO₂-C₃H₆-(30%)NH₂

(10.1 mole/sec. $\cdot 10^{-5}$) > Raney nickel (4.8 mole/sec. $\cdot 10^{-5}$) [51] > 5 wt.% Pd/C (4.4 mole/sec. $\cdot 10^{-5}$) \approx 5 wt.% Pd/ γ -Al₂O₃ (4.4 mole/sec. $\cdot 10^{-5}$) > 5 wt.% Pd/SiO₂ (0.8 mole/sec. $\cdot 10^{-5}$) (Figure 7, Table 4).

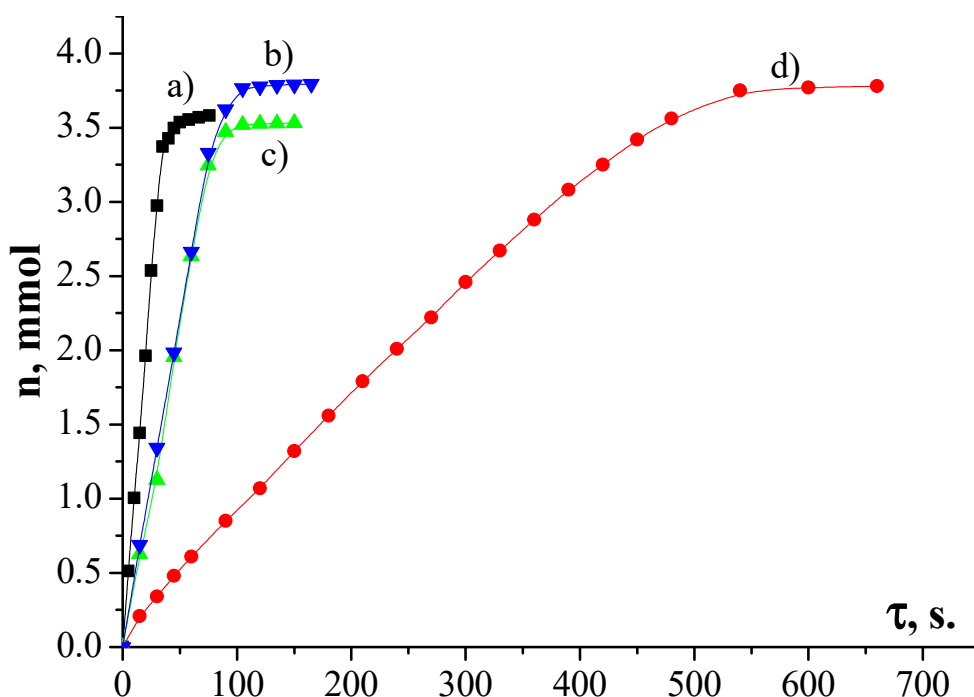


Figure 7. Kinetic curves of hydrogen uptake in the 4-nitroaniline hydrogenation in aqueous 2-propanol (0.68 mol fraction). $T = 298\text{K}$, $m_{\text{(cat)}} = 0.30 \pm 0.05 \text{ g.}$, $m_{\text{(NA)}} = 0.50 \pm 0.05 \text{ g.}$ (a) 5 wt.% Pd/SiO₂-C₃H₆-(30%)NH₂; (b) 5 wt.% Pd/C; (c) 5 wt.% Pd/ γ -Al₂O₃; (d) 5 wt.% Pd/SiO₂.

Table 4. Catalytic recyclability test for a successive five cycles of 4-nitroaniline hydrogenation.

Catalyst	The Hydrogen Consumption Rate $10^{-5} \text{ Mole(H}_2\text{)}/\text{sec.}$				
	1 run	2 run	3 run	4 run	5 run
5 wt.% Pd/SiO ₂ -C ₃ H ₆ -(30%)NH ₂	10.1	9.5	8.8	8.3	8.0
5 wt.% Pd/SiO ₂ [45,52]	0.8	0.8	0.8	0.7	0.6

A drastic increase in the catalytic activity for Pd/SiO₂-C₃H₆-(30%)NH₂ sample compared to Pd/SiO₂ can be subscribed to an increase in the active surface as a result of some decrease in Pd nanoparticles' average diameter. However, Pd nanoparticles' surface modification by aminogroups and a shift in electron density to Pd nanoparticles can be the main reason for the increase in Pd activity [24,46,47].

Comparison of the catalysts' activity after a catalyst recycle showed that the highest activity after five reaction cycles was observed for 5 wt.% Pd/SiO₂-C₃H₆-(30%)NH₂ (Table 4, Figure 7). The catalysts' stability can be arranged in the following order: 5 wt.% Pd/SiO₂-C₃H₆-(30%)NH₂ > 5 wt.% Pd/SiO₂ > 5 wt.% Pd/C \approx 5 wt.% Pd/ γ -Al₂O₃.

Gas chromatographic analysis made it possible to calculate the yield of 1,4-phenylenediamine in the hydrogenation reaction after each repeated addition of 4-nitroaniline (Table 5). In all samples, at the end of the reaction, in each input of 4-nitroaniline, traces of the initial compound were not detected, and the hydrogenation conversion of 4-nitroaniline was considered to be close to full conversion.

Analysis of 4-nitroaniline conversion rate and the formation of 1,4-phenylenediamine showed a similar tendency to decrease in the values of the rates, as for the consumption of hydrogen (Table 4).

Table 5. Data of gas chromatographic analysis in hydrogenation of 4-nitroaniline to 1,4-phenylenediamine.

Catalyst	Conversion * of 4-nitroaniline	Yields * of 1,4-phenylenediamine
5 wt.% Pd/SiO ₂ -C ₃ H ₆ -(30%)NH ₂	100	100
5 wt.% Pd/C	100	100
5 wt.% Pd/SiO ₂	100	100
5 wt.% Pd/ γ -Al ₂ O ₃	100	100

* in each reaction cycle.

The second catalyst with a lower content of amino groups was obtained to confirm the effect of the number of amino groups on the surface.

A kinetic experiment showed that the activity of the 5 wt.% Pd/SiO₂-C₃H₆-(30%)NH₂ catalyst with an NH₂ content of 30 wt.% is two times higher than the 5 wt.% Pd/SiO₂-C₃H₆-(10%)NH₂ catalyst with a content of 10 wt.% NH₂ groups: $10.1 \cdot 10^{-5}$ mole (H₂)/sec and $5.5 \cdot 10^{-5}$ mole (H₂)/sec. Kinetic curves of the hydrogen uptake of the catalytic hydrogenation of 4-nitroaniline on organically modified catalysts are shown in Figure 8. The higher the concentration of amino groups on the matrix surface was fixed, the more active the palladium deposited on the silica matrix [24,46,47].

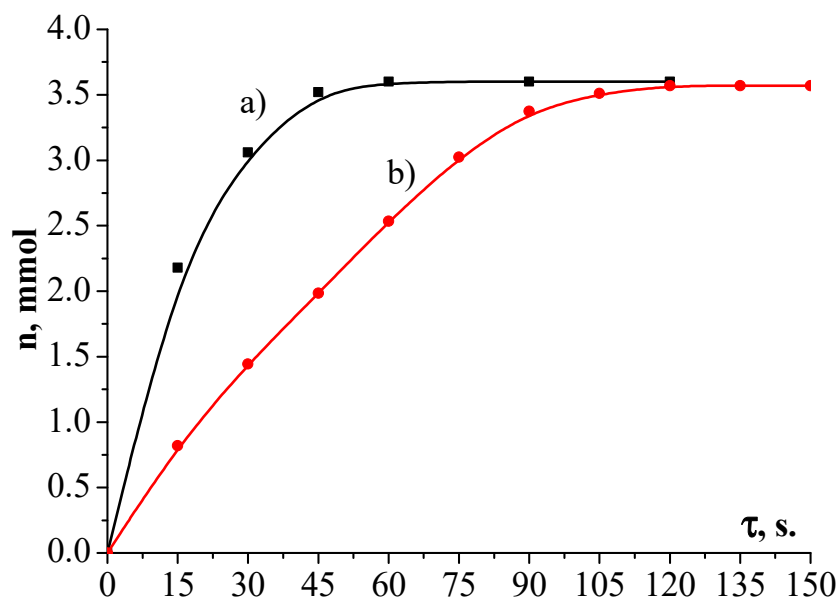


Figure 8. Kinetic curves of hydrogen uptake in the 4-nitroaniline hydrogenation in aqueous 2-propanol (0.68 mol fraction). T = 298K, $m_{\text{(cat)}} = 0.30 \pm 0.05$ g., $m_{\text{(NA)}} = 0.50 \pm 0.05$ g. (a) 5 wt.% Pd/SiO₂-C₃H₆-(30%)NH₂; (b) 5 wt.% Pd/SiO₂-C₃H₆-(10%)NH₂.

According to gas chromatography analysis, the conversion of 4-nitroaniline and the yield of 1,4-phenylenediamine also amounted to 100%.

3. Materials and Methods

3.1. Chemicals and Materials

Tetraethoxysilane (99.9 wt.% Vecton, St. Petersburg, Russia), 2-propanol (99 wt.% Vecton, St. Petersburg, Russia) aminopropyltrimetoxysilane (97 wt.%, Sigma Aldrich, Hamburg, Germany), dodecyldimethylamine N-oxide (30 wt.% solution in water, Sigma Aldrich, Saint-Quentin-Fallavier, France), Cyclohexane (99 wt.%, ECOS-1, Moscow, Russia), sodium carbonate (Vecton, St. Petersburg, Russia), hydrochloric acid (Vecton, St. Petersburg, Russia), palladium chloride (PdCl₂·2H₂O, JSC “Aurat”, Moscow, Russia), aqueous ammonia solution (60 wt.%, Vecton, St. Petersburg, Russia) the

high-purity gases (H_2 99.998%, Ar 99.99%) for the catalyst synthesis were used. The γ - Al_2O_3 and activated carbon ARD-2 were purchased from Reachim Ltd. Russia and were used for catalyst synthesis as received.

3.2. Sol-Gel Method

3.2.1. Synthesis of Silica

To synthesize spherical silica nanoparticles, 700 mL of distilled water was added to 500 mL of 2-propanol in a flat-bottomed flask and the solution was stirred to obtain a uniform solution. Then, 200 mL of tetraethoxysilane was added to the solution. The reaction mixture was kept under vigorous stirring for 30 min with a mixing rate of 1500 rpm. Subsequently, 50 mL of aqueous ammonia solution (60 wt.%) was added dropwise to the reaction mixture over 30 min. The mixture was stirred for 2 h with a mixing rate of 1000 rpm. Then, the precipitate was filtered, washed with distilled water and dried at 200 °C for 3 h on air.

3.2.2. Synthesis of Amino-Functionalized Silica

The first step of the reaction procedure was to prepare the oil/water emulsion. For this, 104 mL of distilled water and 16 mL of pure ethanol were mixed with a stirrer with a mixing rate 1500 rpm. Then, 2 mL of cyclohexane was added as a co-template. After the addition of 4.8 mL of dodecyldimethylamine N-oxide to the solution, the formation of emulsion was observed. To achieve a higher emulsion dispersion, the mixture was treated by ultrasound for 5 min in ultrasonic bath 36–42 kHz, 200 W. In order to homogenize the reaction mixture, an extra 0.2 mL of surfactant was added. Then, 0.8 mL for SiO_2 - C_3H_6 -(30%) NH_2 and 0.3 mL for SiO_2 - C_3H_6 -(10%) NH_2 of aminopropyltrimetoxysilane were adjusted in the system for particles' formation. The solution was stirred for 10 min at a reaction temperature 60 °C. Then first portion of tetraethoxysilane (1 mL) was added to the mixture and solution opalescence was immediately observed. The solution was stirred for 24 h at room temperature. The final solution was a viscous colloid of white color, which was sufficiently stable. A vacuum filtration of solution with 0.2 micrometers membrane filter was used to separate the dispersed phase from the solution. The material was dried in vacuum oven at pressure of 0.4 bar and temperature of 100 °C.

3.3. Catalyst Preparation

The synthesis of Pd-based catalysts was made by the precipitation of palladium hydroxide due to hydrolysis reaction by the addition of 3 mM H_2PdCl_4 solution in water to 1g of support (SiO_2 , γ - Al_2O_3 or activated carbon) suspended in a 40 mL aqueous solution of 0.1 M Na_2CO_3 and 0.1M solution of sodium dodecyl sulfate using an ultrasonic bath (Bandelin, 10P, Mannheim, Germany). The solution of H_2PdCl_4 was prepared in 0.2 M hydrochloric acid. The suspension was mixed for 3 h at 35 °C in an ultrasonic bath. The catalysts sample was filtered, thoroughly washed with distilled water and dried at 65 °C under air. Prior to kinetic experiments, catalysts' sample was reduced at 250 °C for 60 min in the hydrogen flow in tube furnace than cooled to ambient temperature and flashed with nitrogen and immediately transferred to the catalytic reactor. The following samples were synthesized by this methodology and denoted as 5 wt.% Pd/ γ - Al_2O_3 , 5 wt.% Pd/ SiO_2 , 5 wt.% Pd/C, 5 wt.% Pd/ SiO_2 - C_3H_6 - NH_2 , with an NH_2 content of 30 wt.%.

3.4. Catalyst Characterization

3.4.1. Fourier Transform Infrared Spectroscopy (FTIR)

The diffuse reflectance IR spectroscopy was carried out using the FTIR spectrometer IRPrestige-21 (Shimadzu, Kyoto, Japan) equipped with a diffuse reflection attachment. DRS-8000 was used for the

qualitative composition of catalyst surface. The resolution of all spectra was 4 cm^{-1} and spectra were registered in the wave number range $490\text{--}4000\text{ cm}^{-1}$.

3.4.2. Hydrogen Pulse Chemisorption

The metal dispersion and the chemically active surface area were determined due to pulse chemisorption analysis by applying a pulsed titration of the catalyst with a hydrogen. The spectra were registered on an automatic analyzer of chemisorption AutoChem HP 2950 (Micromeritics, Norcross, GA, USA).

3.4.3. XPS

X-ray photoelectron spectroscopy (XPS) data were obtained using ES-2403 spectrometer (manufacturer: Institute for Analytic Instrumentation of RAS, St. Petersburg, Russia) with anode Mg $K\alpha$ ($h\nu = 1253.6\text{ eV}$), energy analyzer PHOIBOS 100-MCD5 (SPECS, Berlin, Germany) and X-Ray source XR-50 (SPECS, Berlin, Germany). All the data were acquired at an X-ray power of 250 W. Survey spectra were recorded at an energy step of 0.5 eV with the analyzer pass energy 40 eV, and high resolution spectra were recorded at an energy step of 0.05 eV with the analyzer pass energy 7 eV. Samples were degassed within 180 min before analysis and were stable during the treatment. The obtained spectra were analyzed using CasaXPS software taking sensitivity factors in the quantity analysis of data into account.

3.4.4. SEM

The morphological characteristics of the amino-functionalized mesoporous silica and catalyst were examined by scanning electron microscopy (SEM, TESCAN, Vega-LSU) equipped with X-ray microanalysis (OXFORD INCA PentaFETx3). Scanning electron microscope images were acquired at a magnification of 66.1 kX at 20 kV with an SE detector.

3.4.5. TEM

The structural properties of the samples were examined using an electron microscope (JEM-2200FS, accelerating voltage 200 kV) in the transmission high-resolution electron microscopy mode (PFEM, high-resolution transmission electron microscopy—HRTEM). A model of the microscope JEOL JEM-2200FS showed an accelerating voltage of 200 kV. Resolution: by points—0.19 nm; on the lattice—0.1 nm; in the mapping mode—0.2 nm; in the HAADF mode—0.14 nm. For the analysis of the elemental composition, electron microscopy was used in the energy dispersive X-ray spectroscopy mode (EMF, energy-dispersive X-ray spectroscopy (EDS)).

3.4.6. Temperature Programmed Desorption (TPD) of NH_3

The study of support acid properties was provided by AutoChem HP 2950 automatic chemisorption analyzer (Micromeritics, Norcross, GA, USA). The high purity grade helium was used by way of carrier gas. The signal was recorded by a heat conductivity detector. The studied sample was pre-processed in mixture 3% NH_3 -He flow at room temperature. The excess of NH_3 gas was desorbed by flushing the system with helium upon gradual heating with a rate of $10\text{ }^\circ\text{C}/\text{min}$. The desorption of NH_3 was carried by heating the sample up to $950\text{ }^\circ\text{C}$ with a constant heating rate of $10\text{ }^\circ\text{C}$ per minute. Then, the sample was cooled to ambient temperature.

3.4.7. Catalysts Activity Experiments Description

The stirred reactor with the temperature-control was used to carry out 4-nitroaniline hydrogenation to 1,4-phenylenediamine. The catalysts 5 wt.% Pd/ $\text{SiO}_2\text{-C}_3\text{H}_6\text{-NH}_2$, 5 wt.% Pd/ SiO_2 , 5 wt.% Pd/ $\gamma\text{-Al}_2\text{O}_3$ and 5 wt.% Pd/C were tested in the hydrogenation of 4-nitroaniline in the environment of a water solution of 2-propanol (0.68 mole fraction). Before experiments, the reactor was flushed three times with

hydrogen for air removal. The reaction rates were defined by volumetric measurements of hydrogen consumption. The rates of reaction were calculated as an inclination angle tangent of kinetic curves of hydrogen consumption. The test for the contribution of homogeneous catalysis to the reaction rate was performed by Sheldon's filtration test methodology. After the partial conversion of 4-nitroaniline, the reaction stopped and the catalyst was extracted by filtration. Further to this, the reaction was continued without catalyst, but chemical transformation wasn't observed. Thus, the hydrogenation was catalyzed only by heterogeneous catalysts.

Chromatographic analysis was performed using a gas chromatograph (Crystal, manufacturer Chromatek, Yoshkar-Ola, Russia). The reaction rate was controlled through the 4-nitroaniline conversion. After completion, the catalyst was separated from the reaction mixture by centrifugation.

3.4.8. Deactivation Experiments Using Recovered Catalysts

The deactivation of catalysts was studied by the hydrogenation of 4-nitroaniline to 1,4-phenylenediamine in a water solution of 2-propanol with the repeated injection of 4-nitroaniline at the end of reaction. Five repeated injections of 4-nitroaniline were carried out on each catalyst.

4. Conclusions

Silica surface modification with aminopropyltrimetoxysilane allows the effective synthesis of catalytically active Pd nanoparticles with diameters varying from 3 to 10 nm. Pd species mainly present in the form of metal palladium and palladium oxide(II). Silica surface modification with amino groups results in a higher palladium surface concentration (2.12 at%) compared to unmodified silica (1.47 at%) according to XPS data. This results in an increase in sample activity in p-nitroaniline hydrogenation reaction up to $10.1 \text{ mole(H}_2\text{)/sec} \cdot 10^{-5}$ for 5 wt.% Pd/SiO₂-C₃H₆-(30%)NH₂ compared to $0.8 \text{ mole(H}_2\text{)/sec} \cdot 10^{-5}$ for the unmodified sample 5 wt.% Pd/SiO₂.

The comparison of TPD and kinetics data shows a certain correlation. The higher the acidity of the support, the higher the activity of supported palladium.

An increase in surface aminogroups concentration in the case of samples 5 wt.% Pd/SiO₂-C₃H₆-(30%)NH₂ and 5 wt.% Pd/SiO₂-C₃H₆-(10%)NH₂ results in an appropriate increase in catalytic activity by 1.9 times. This confirms the hypothesis that the electron-donating properties of the amino group have a positive effect on the catalytic activity of the supported metal. This also confirms the kinetic experiments using an unmodified, commonly used Pd supported on activated carbon, alumina and Raney nickel samples. Silica surface modification with amino aminopropyltrimetoxysilane has a positive influence on catalyst stability because of palladium nanoparticles' strong interaction with silica compare to unmodified support.

Author Contributions: Conceptualization, E.V.R.; Formal analysis, A.R.L., E.V.R., D.V.F. and A.V.B.; Investigation, A.R.L., M.D.L. and A.V.B.; Methodology, D.V.F.; Project administration, E.V.R. and O.V.L.; Supervision, V.Y.D.; Visualization, A.R.L.; Writing—original draft, A.R.L. and D.V.F.; Writing—review & editing, V.Y.D. All authors have read and agreed to the published version of the manuscript.

Funding: The work was funded by the Russian Science Foundation Grant No. 18-79-10157.

Conflicts of Interest: The authors declare no conflicts of interest.

References

1. Gómez, J.E.; Kleij, A.W. Chapter Three-Catalytic nonreductive valorization of carbon dioxide into fine chemicals. In *Advances in Organometallic Chemistry*; Pérez, P.J., Ed.; Academic Press: Cambridge, MA, USA, 2019; Volume 71, pp. 175–226. [[CrossRef](#)]
2. Gabriele, B. Chapter 3-Synthesis of Heterocycles by Palladium-Catalyzed Carbonylative Reactions. In *Advances in Transition-Metal Mediated Heterocyclic Synthesis*; Solé, D., Fernández, I., Eds.; Academic Press: Cambridge, MA, USA, 2018; pp. 55–127. [[CrossRef](#)]
3. Masuda, K.; Ichitsuka, T.; Koumura, N.; Sato, K.; Kobayashi, S. Flow fine synthesis with heterogeneous catalysts. *Tetrahedron* **2018**, *74*, 1705–1730. [[CrossRef](#)]

4. Yokoi, T.; Kubota, Y.; Tatsumi, T. Amino-functionalized mesoporous silica as base catalyst and adsorbent. *Appl. Catal. A Gen.* **2012**, *421*, 14–37. [\[CrossRef\]](#)
5. Hocking, M.B. 19-PETROCHEMICALS. In *Handbook of Chemical Technology and Pollution Control*; Hocking, M.B., Ed.; Academic Press: San Diego, CA, USA, 1998; pp. 633–664. [\[CrossRef\]](#)
6. Speight, J.G. Chapter 3-Industrial Organic Chemistry. In *Environmental Organic Chemistry for Engineers*; Speight, J.G., Ed.; Butterworth-Heinemann: Oxford, UK, 2017; pp. 87–151. [\[CrossRef\]](#)
7. Védérine, J.C. 8-Main industrial processes using metal oxides as catalysts or support and future trends in heterogeneous catalysis. In *Metal Oxides in Heterogeneous Catalysis*; Védérine, J.C., Ed.; Elsevier: Amsterdam, The Netherlands, 2018; pp. 401–549. [\[CrossRef\]](#)
8. Kelkar, A.A. Chapter 14-Carbonylations and Hydroformylations for Fine Chemicals. In *Industrial Catalytic Processes for Fine and Specialty Chemicals*; Joshi, S.S., Ranade, V.V., Eds.; Elsevier: Amsterdam, The Netherlands, 2016; pp. 663–692. [\[CrossRef\]](#)
9. Borah, B.J.; Mondal, M.; Bharali, P. Chapter 27-Palladium-Based Hybrid Nanocatalysts: Application toward Reduction Reactions. In *Noble Metal-Metal Oxide Hybrid Nanoparticles*; Mohapatra, S., Nguyen, T.A., Nguyen-Tri, P., Eds.; Woodhead Publishing: Cambridge, UK, 2019; pp. 565–583. [\[CrossRef\]](#)
10. Albéniz, A.C.; Casares, J.A. Chapter One-Palladium-Mediated Organofluorine Chemistry. In *Advances in Organometallic Chemistry*; Pérez, P.J., Ed.; Academic Press: Cambridge, MA, USA, 2014; Volume 62, pp. 1–110. [\[CrossRef\]](#)
11. Zhang, R.; Xue, M.; Wang, B.; Ling, L. Acetylene selective hydrogenation over different size of Pd-modified Cu cluster catalysts: Effects of Pd ensemble and cluster size on the selectivity and activity. *Appl. Surf. Sci.* **2019**, *481*, 421–432. [\[CrossRef\]](#)
12. Yang, Q.; Hou, R.; Sun, K. Tuning butene selectivities by Cu modification on Pd-based catalyst for the selective hydrogenation of 1, 3-butadiene. *J. Catal.* **2019**, *374*, 12–23. [\[CrossRef\]](#)
13. Eslava, J.L.; Gallegos-Suárez, E.; Guerrero-Ruiz, A.; Rodríguez-Ramos, I. Effect of Mo promotion on the activity and selectivity of Ru/Graphite catalysts for Fischer-Tropsch synthesis. *Catal. Today* **2019**. [\[CrossRef\]](#)
14. He, Z.-H.; Li, N.; Wang, K.; Wang, W.-T.; Liu, Z.-T. Selective hydrogenation of quinolines over a CoCu bimetallic catalyst at low temperature. *Mol. Catal.* **2019**, *470*, 120–126. [\[CrossRef\]](#)
15. Chakoli, A.N.; Sadeghzadeh, M. Chapter 27-Recent Trends in Biomedical and Pharmaceutical Industry Due to Engineered Nanomaterials. In *Handbook of Nanomaterials for Industrial Applications*; Mustansar Hussain, C., Ed.; Elsevier: Amsterdam, The Netherlands, 2018; pp. 499–519. [\[CrossRef\]](#)
16. Zhu, J.; Wood, J.; Deplanche, K.; Mikheenko, I.; Macaskie, L.E. Selective hydrogenation using palladium bioinorganic catalyst. *Appl. Catal. B Environ.* **2016**, *199*, 108–122. [\[CrossRef\]](#)
17. Akti, F. The effect of potassium modification on structural properties and catalytic activity of copper and iron containing SBA-16 catalysts for selective oxidation of ethanol. *Mater. Chem. Phys.* **2019**, *227*, 21–28. [\[CrossRef\]](#)
18. Sánchez, G.; Friggieri, J.; Keast, C.; Drewery, M.; Długogorski, B.Z.; Kennedy, E.; Stockenhuber, M. The effect of catalyst modification on the conversion of glycerol to allyl alcohol. *Appl. Catal. B Environ.* **2014**, *152*, 117–128. [\[CrossRef\]](#)
19. Zhang, H.; Ke, D.; Cheng, L.; Feng, X.; Hou, X.; Wang, J.; Li, Y.; Han, S. CoPt-Co hybrid supported on amino modified SiO₂ nanospheres as a high performance catalyst for hydrogen generation from ammonia borane. *Prog. Nat. Sci. Mater. Int.* **2019**, *29*, 1–9. [\[CrossRef\]](#)
20. Fernandes, A.E.; Jonas, A.M. Design and engineering of multifunctional silica-supported cooperative catalysts. *Catal. Today* **2018**, *334*, 173–186. [\[CrossRef\]](#)
21. Feng, X.; Song, Z.; Guo, T.; Yang, R.; Liu, Y.; Chen, X.; Yang, C. Insights into the effect of surface functional groups on catalytic performance for hydrogen generation from sodium borohydride. *RSC Adv.* **2016**, *6*, 113260–113266. [\[CrossRef\]](#)
22. Khalili, D.; Banazadeh, A.R.; Etemadi-Davan, E. Palladium Stabilized by Amino-Vinyl Silica Functionalized Magnetic Carbon Nanotube: Application in Suzuki-Miyaura and Heck-Mizoroki Coupling Reactions. *Catal. Lett.* **2017**, *147*, 2674–2687. [\[CrossRef\]](#)
23. Miller, J.T.; Mojet, B.L.; Ramaker, D.E.; Koningsberger, D.C. A new model for the metal-support interaction: Evidence for a shift in the energy of the valence orbitals. *Catal. Today* **2000**, *62*, 101–114. [\[CrossRef\]](#)

24. Jin, M.-H.; Park, J.-H.; Oh, D.; Park, J.-S.; Lee, K.-Y.; Lee, D.-W. Effect of the amine group content on catalytic activity and stability of mesoporous silica supported Pd catalysts for additive-free formic acid dehydrogenation at room temperature. *Int. J. Hydrogen Energy* **2019**, *44*, 4737–4744. [\[CrossRef\]](#)
25. Vona, D.; Cicco, S.; Ragni, R.; Leone, G.; Lo Presti, M.; Farinola, G. Biosilica/polydopamine/silver nanoparticles composites: New hybrid multifunctional heterostructures obtained by chemical modification of *Thalassiosira weissflogii* silica shells. *MRS Commun.* **2018**, *8*, 911–917. [\[CrossRef\]](#)
26. Gupta, R.K.; Kusuma, D.Y.; Lee, P.S.; Srinivasan, M.P. Covalent Assembly of Gold Nanoparticles for Nonvolatile Memory Applications. *ACS Appl. Mater. Interfaces* **2011**, *3*, 4619–4625. [\[CrossRef\]](#)
27. Alvarez-Toral, A.; Fernández, B.; Malherbe, J.; Claverie, F.; Pecheyran, C.; Pereiro, R. Synthesis of amino-functionalized silica nanoparticles for preparation of new laboratory standards. *Spectrochim. Acta Part B At. Spectrosc.* **2017**, *138*, 1–7. [\[CrossRef\]](#)
28. Sugimura, H.; Hanji, T.; Takai, O.; Masuda, T.; Misawa, H. Photolithography based on organosilane self-assembled monolayer resist. *Electrochim. Acta* **2001**, *47*, 103–107. [\[CrossRef\]](#)
29. Pasquardini, L.; Lunelli, L.; Potrich, C.; Marocchi, L.; Fiorilli, S.; Vozzi, D.; Vanzetti, L.; Gasparini, P.; Anderle, M.; Pederzoli, C. Organo-silane coated substrates for DNA purification. *Appl. Surf. Sci.* **2011**, *257*, 10821–10827. [\[CrossRef\]](#)
30. Oliveira, R.L.; He, W.; Klein Gebbink, R.J.M.; de Jong, K.P. Palladium nanoparticles confined in thiol-functionalized ordered mesoporous silica for more stable Heck and Suzuki catalysts. *Catal. Sci. Technol.* **2015**, *5*, 1919–1928. [\[CrossRef\]](#)
31. Hajipour, A.R.; Mohammadsaleh, F. Triazole-Functionalized Silica Supported Palladium(II) Complex: A Novel and Highly Active Heterogeneous Nano-catalyst for C–C Coupling Reactions in Aqueous Media. *Catal. Lett.* **2018**, *148*, 1035–1046. [\[CrossRef\]](#)
32. Yuan, M.; Yang, R.; Wei, S.; Hu, X.; Xu, D.; Yang, J.; Dong, Z. Ultra-fine Pd nanoparticles confined in a porous organic polymer: A leaching-and-aggregation-resistant catalyst for the efficient reduction of nitroarenes by NaBH₄. *J. Colloid Interface Sci.* **2019**, *538*, 720–730. [\[CrossRef\]](#) [\[PubMed\]](#)
33. Bourane, A.; Elanany, M.; Pham, T.V.; Katikaneni, S.P. An overview of organic liquid phase hydrogen carriers. *Int. J. Hydrogen Energy* **2016**, *41*, 23075–23091. [\[CrossRef\]](#)
34. Schrimpf, M.; Esteban, J.; Rösler, T.; Vorholt, A.J.; Leitner, W. Intensified reactors for gas-liquid-liquid multiphase catalysis: From chemistry to engineering. *Chem. Eng. J.* **2019**, *372*, 917–939. [\[CrossRef\]](#)
35. Song, J.; Huang, Z.-F.; Pan, L.; Li, K.; Zhang, X.; Wang, L.; Zou, J.-J. Review on selective hydrogenation of nitroarene by catalytic, photocatalytic and electrocatalytic reactions. *Appl. Catal. B Environ.* **2018**, *227*, 386–408. [\[CrossRef\]](#)
36. Huang, T.; Fu, Y.; Peng, Q.; Yu, C.; Zhu, J.; Yu, A.; Wang, X. Catalytic hydrogenation of p-nitrophenol using a metal-free catalyst of porous crimped graphitic carbon nitride. *Appl. Surf. Sci.* **2019**, *480*, 888–895. [\[CrossRef\]](#)
37. Sharma, S. Metal dependent catalytic hydrogenation of nitroarenes over water-soluble glutathione capped metal nanoparticles. *J. Colloid Interface Sci.* **2015**, *441*, 25–29. [\[CrossRef\]](#)
38. Fu, Y.; Qin, L.; Huang, D.; Zeng, G.; Lai, C.; Li, B.; He, J.; Yi, H.; Zhang, M.; Cheng, M.; et al. Chitosan functionalized activated coke for Au nanoparticles anchoring: Green synthesis and catalytic activities in hydrogenation of nitrophenols and azo dyes. *Appl. Catal. B Environ.* **2019**, *255*, 117740. [\[CrossRef\]](#)
39. Zarrintaj, P.; Bakhshandeh, B.; Saeb, M.R.; Sefat, F.; Rezaeian, I.; Ganjali, M.R.; Ramakrishna, S.; Mozafari, M. Oligoaniline-based conductive biomaterials for tissue engineering. *Acta Biomater.* **2018**, *72*, 16–34. [\[CrossRef\]](#)
40. Amer, I.; Mokrani, T.; Jewell, L.; Young, D.A.; Vosloo, H.C.M. Oxidative copolymerization of p-phenylenediamine and 3-aminobenzenesulfonic acid. *Tetrahedron Lett.* **2016**, *57*, 426–430. [\[CrossRef\]](#)
41. Jin, J.-S.; Ning, Y.-Y.; Hu, K.; Wu, H.; Zhang, Z.-T. Solubility of p-Nitroaniline in Supercritical Carbon Dioxide with and without Mixed Cosolvents. *J. Chem. Eng. Data* **2013**, *58*, 1464–1469. [\[CrossRef\]](#)
42. Nishioka, R.; Hiasa, T.; Kimura, K.; Onishi, H. Specific Hydration on p-Nitroaniline Crystal Studied by Atomic Force Microscopy. *J. Phys. Chem. C* **2013**, *117*, 2939–2943. [\[CrossRef\]](#)
43. Scaffaro, R.; Botta, L.; Lo Re, G.; Bertani, R.; Milani, R.; Sassi, A. Surface modification of poly(ethylene-co-acrylic acid) with amino-functionalized silica nanoparticles. *J. Mater. Chem.* **2011**, *21*, 3849–3857. [\[CrossRef\]](#)
44. Jakša, G.; Štefane, B.; Kovač, J. XPS and AFM characterization of aminosilanes with different numbers of bonding sites on a silicon wafer. *Surf. Interface Anal.* **2013**, *45*, 1709–1713. [\[CrossRef\]](#)

45. Latypova, A.; Tarasyuk, I.; Filippov, D.; Lefedova, O.; Bykov, A.; Sidorov, A.; Doluda, V.; Sulman, E. Synthesis, stability and activity of palladium supported over various inorganic matrices in the selective hydrogenation of nitroaniline. *React. Kinet. Mech. Catal.* **2019**, *127*, 741–755. [[CrossRef](#)]
46. Li, L.; Zhao, H.; Wang, J.; Wang, R. Facile Fabrication of Ultrafine Palladium Nanoparticles with Size- and Location-Control in Click-Based Porous Organic Polymers. *ACS Nano* **2014**, *8*, 5352–5364. [[CrossRef](#)]
47. Zhong, H.; Liu, C.; Wang, Y.; Wang, R.; Hong, M. Tailor-made porosities of fluorene-based porous organic frameworks for the pre-designable fabrication of palladium nanoparticles with size, location and distribution control. *Chem. Sci.* **2016**, *7*, 2188–2194. [[CrossRef](#)]
48. Zhang, D.; Jin, C.; Tian, H.; Xiong, Y.; Zhang, H.; Qiao, P.; Fan, J.; Zhang, Z.; Li, Z.Y.; Li, J. An In situ TEM study of the surface oxidation of palladium nanocrystals assisted by electron irradiation. *Nanoscale* **2017**, *9*, 6327–6333. [[CrossRef](#)]
49. Chen, A.; Ostrom, C. Palladium-Based Nanomaterials: Synthesis and Electrochemical Applications. *Chem. Rev.* **2015**, *115*, 11999–12044. [[CrossRef](#)]
50. Blosi, M.; Ortelli, S.; Costa, A.L.; Dondi, M.; Lolli, A.; Andreoli, S.; Benito, P.; Albonetti, S. Bimetallic Nanoparticles as Efficient Catalysts: Facile and Green Microwave Synthesis. *Materials* **2016**, *9*, 550. [[CrossRef](#)] [[PubMed](#)]
51. Kha, N.T.T.; Merkin, A.A.; Komarov, A.A.; Korpatenkov, D.O.; Lefedova, O.V. Kinetics of catalytic hydrogenation of 4-nitroaniline in aqueous solutions of propan-2-ol with acid or base additives. *Russ. J. Phys. Chem. A* **2014**, *88*, 588–590. [[CrossRef](#)]
52. Doluda, V.Y.; Sidorov, A.I.; Sulman, E.M.; Latypova, A.R.; Filippov, D.V.; Lefedova, O.V. Synthesis, structure and catalytic properties of Pd nanostructured materials in p-nitroaniline catalytic hydrogenation. *Izv. Vyssh. Uchebnykh Zaved. Khimiya Khimicheskaya Tekhnol.* **2019**, *62*, 60–68. [[CrossRef](#)]



© 2020 by the authors. Licensee MDPI, Basel, Switzerland. This article is an open access article distributed under the terms and conditions of the Creative Commons Attribution (CC BY) license (<http://creativecommons.org/licenses/by/4.0/>).